DETECTING WATER BODIES ON RADARSAT IMAGERY

Gangyao Kuang, and Zhiguo He, School of Electronics Science and Engineering,
National University of Defense Technology, China
Jonathan Li, Department of Geography and Environmental Management,
University of Waterloo, Waterloo, Ontario

This paper presents a novel geodesic active contour (GAC) model based on an edge detector for rapid detection of water bodies from spaceborne synthetic aperture radar (SAR) imagery with high speckle noise. The original edge indicator function based on gradients is replaced by an edge indicator function based on the ratio of exponentially weighted averages (ROEWA) operator. Thus, the capability of edge detection and the accuracy of locating edges are greatly improved, which makes the model more appropriate for SAR images. In addition, an enhancing term is added to the original model's energy function in order to boost the strength for the contour's evolution. An unconditionally stable additive operator splitting (AOS) scheme and a fast algorithm for re-initialization of the level set function are adopted, which not only enhances the model's stability, but also speeds up the model's convergence remarkably. The experimental results on simulated and real RADARSAT-1/-2 images show its efficiency and accuracy.

Cet article présente un nouveau modèle de contour actif géodésique (GAC, de l'anglais geodesic active contour) fondé sur un détecteur de contours pour détection rapide des plans d'eau à partir d'images radar à synthèse d'ouverture (RSO) spatioporté avec bruits de chatoiement élevés. La fonction originale d'indicateur de contours fondée sur les gradients est remplacée par une fonction d'indicateur de contours fondée sur le rapport d'un opérateur de moyennes pondérées de façon exponentielle (ROEWA). Par conséquent, la capacité de détection des contours et l'exactitude des contours localisés sont grandement améliorées, ce qui rend le modèle plus adéquat pour les images RSO. De plus, une modalité d'amélioration s'ajoute à la fonction d'énergie du modèle original dans le but de renforcir la puissance de l'évolution des contours. On a adopté un scénario de séparation d'opérateur additif (SOA) inconditionnellement stable et un algorithme rapide pour la réinitialisation des surfaces de niveau, ce qui non seulement améliore la stabilité du modèle, mais accélère aussi la convergence du modèle de façon remarquable. Les résultats expérimentaux sur des images simulées et réelles RADARSAT-1/-2 démontrent son efficience et son exactitude.

Gangyao Kuang

Jonathan Li
junli@uwaterloo.ca

Zhiguo He

1. Introduction

Wa ... a a ... a ... a, a a a a a, ... a a a, a a a ... D a b ... a a, a O a, Ca a a, a - a b a b. Ea b a a a a b - a a a (SAR) a, a, a a a b a a a a a (. ., a , a) a (b) a a a a (. ., a a a a,) [*Shultz and Engman* 2000]. SAR a a a ab a a b , a a a a .T a a a b a a a a-

a a ab a a a- a a a a a a a a .H SAR a a a a . I a a a SAR a a a - a a . I a , a a a a b a a a a . A , - a b , a , -ba [*Oliver et al*. 1996; *Collins and Kopp* 2008], Ma a (MRF) [*Fjortoft et al*. 2003], [*Shu et al.* 2010], a / a [*Cook et al*. 1994]. T -ba a a b a a , a a .

T a ba a
a a . H , a b
a -ba a
b a a a a a a
a
a a a [*He* 2009]. T
MRF a
a a b
a a a a a
a a a a . H , MRF
a a a b a -
a a a , a a a a -
a b . T a ba
a b *Shu et al*. [2010]
b a -
SAR a a a a
b a
. T ,
a (MUM) [*Cook*
a . 1994], a a a
a . A
a a ab a
a a a
a a . B ,
a a a a a a
I a , a ba
a a a
[*Kass et al*. 1988; *Cohen* 1991; *Sethian* 1996; *Zhu and Yuille* 1996; *Caselles et al*. 1997; *Osher and Sethian* 1998]. A a -
a b *Kass et al*. [1998].
T a a a a b
a a a
b . T b a -
a a a a a -
a . D -
a a a a
a ab a ba . F
a a a a
a . S , a
a a a a
. T a ba a
b a (GAC)
[*Caselles et al*. 1997]. I , -
a a a a a
R a a . A , a
b a - a
[*Osher and Sethian* 1998]. T a a
a a b ,
a a a -
. H ,
a a b
a SAR a . T a a
b a GAC a a a
a a ba a

SAR a . C a a a
a a a SAR a
a a a a a
: a a
a a a a -
[*Touzi el al*. 1988; *Germain and Refregier* 2001]. H , a SAR
a b . T
a a
a a . *Bovik* [1988] a
Touzi et al [1988]
a a a (ROA). *Fjortoft et al*.
[1998] a a a a
, a
Shen and Castan [1992] - a a
a I a
a a , *Oliver et al*. [1996]
a a , ba
a (LR) . T ROA a LR a
a a a a a
a , a a -
a , a a a
a (ROEWA) a a a -
a - a a a
SAR a . R , a a
[*Chesnaud et al*. 1998, 1999; *Germain and Rfregier* 2001; *Martin et al*. 2004] a
a -
a SAR a . T a -
, b a a a-
. A ab , a
a a a a a a
.
I a , a GAC
ba ROEWA a [*Fjortoft et al*.1998]
a . T a
a a a ba
a a b a a -
ba ROEWA a . T , a a-
b a a a a
a a , a
a a SAR a a . I
a , a ba a -
a a b
. A a ,
. a a -
a . I -
a a , a a -
ab a a (AOS)
[*Weickert et al*. 1998] a a a a - -
a a [*Felzenszwalb and Huttenlocher* 2004] a a ,
. ab , b a
. a ab . T
a a -

a a SAR a . T a a a a . S 2 b ba GAC a a ab SAR a a- . S 3 b ROEWA a a a a GAC . S 4 a a a a a a ba . S 5 a b a a a RADARSAT-1/2SAR a . T a a a b S 6. F a , S 7 .

2. Background

L x b ab a, y b a , $\subset R^2$ b a a , $u_0\ (x, y)$: $\rightarrow R^+$ b a a , C b a a a $L(C)$ a $C(s) = (x(s), y(s))$:[0, $L(C)$] $\rightarrow R^2$ b a - a a a , s a a - a ab . T a a GAC a - a C a b [*Caselles et al.* 1997]

$$\int_0^{L(C)} g\left(\left|\nabla u_0\left(C(s)\right)\right|\right)ds \qquad (1)$$

$\nabla u_0(C(s))$ a a , $\nabla u_0\ (C(s))$ a ( ) a . T a - $g(r)$:[0,) $\rightarrow R^+$ a a - , a $g(0) = 1$ a $g(r) \rightarrow 0$ a , $r \rightarrow$ r a a b a a ab . A a a a a a , a b a a C [*Caselles et al.* 1997]

$$\frac{\partial C}{\partial t} = \left[g\kappa - \langle \nabla g, \vec{n} \rangle \right] \vec{n} \qquad (2)$$

where κ is the mean curvature, $\vec{n}$ is the unit inward a . E . (2) b a a a - a [*Caselles et al.* 1997]. *Osher and Sethian* [1998] a a b a a a a . I a , C a a b a a ϕ, a $C(t) =$ $(x, y) : \phi(x, y, t) = 0$, t a a - ab . B , a a a a a . A , E . (2) a b a [*Caselles et al.* 1997]

$$\frac{\partial \phi}{\partial t} = g\kappa \left| \nabla \phi \right| + \nabla g \cdot \nabla \phi \qquad (3)$$

3. Proposed Model

3.1 ROEWA Operator

T ROEWA a , b *Fjortoft et al.* [1998], ba a a a a (MMSE) I - a (1D) a , a MMSE a b a

$$f\,(x) = C \quad \rho x \qquad (4)$$

C a a , ρ - . I a , $f(x)$ a b b a a a $f_1(x)$ a a a a a $f_2(x)$

$$f(x) = \frac{1}{1+b} = f_1(x) + \frac{b}{1+b} f_2(x-1),\ x = 1, 2, \ldots, N \qquad (5)$$

$f_1(x) = a \cdot b^x\, H(x)$, $f_2(x) = a \cdot b^{-x}\, H(\ x)$, $0 < b = e^{-a} < 1$, $a = 1$ b , $H(x)$ H . I x 0 a , . Ba a MMSE , ROEWA a a b a

$$\begin{cases} r_{X\max}(x,y) = \max\left\{ \dfrac{\hat{\mu}_{X1}(x-1,y)}{\hat{\mu}_{X2}(x+1,y)}, \dfrac{\hat{\mu}_{X2}(x+1,y)}{\hat{\mu}_{X1}(x-1,y)} \right\} \\ r_{Y\max}(x,y) = \max\left\{ \dfrac{\hat{\mu}_{Y1}(x,y-1)}{\hat{\mu}_{Y2}(x,y+1)}, \dfrac{\hat{\mu}_{Y2}(x,y+1)}{\hat{\mu}_{Y1}(x,y-1)} \right\} \end{cases} \qquad (6)$$

where $\hat{\mu}_{X1}, \hat{\mu}_{X2}, \hat{\mu}_{Y1}$ and $\hat{\mu}_{Y2}$ are the exponentially a , a b ba b

$$\begin{cases} \hat{\mu}_{X1}(x,y) = f_1(x) * \left(f(y) \bullet u_0(x,y)\right) \\ \hat{\mu}_{X2}(x,y) = f_2(x) * \left(f(y) \bullet u_0(x,y)\right) \\ \hat{\mu}_{Y1}(x,y) = f_1(y) \bullet \left(f(x) * u_0(x,y)\right) \\ \hat{\mu}_{Y2}(x,y) = f_2(y) \bullet \left(f(x) * u_0(x,y)\right) \end{cases} \qquad (7)$$

* a a • - a . W a a a -ba , a ROEWA a a b a

$$\left| r_{\max}(x,y) \right| = \sqrt{r_{X\max}^2(x,y) + r_{Y\max}^2(x,y)} \qquad (8)$$

F 1 a b a a a RADARSAT-1 a ROEWA a . T b ROEWA a a a b a a . C , ROEWA a a b a a SAR a .

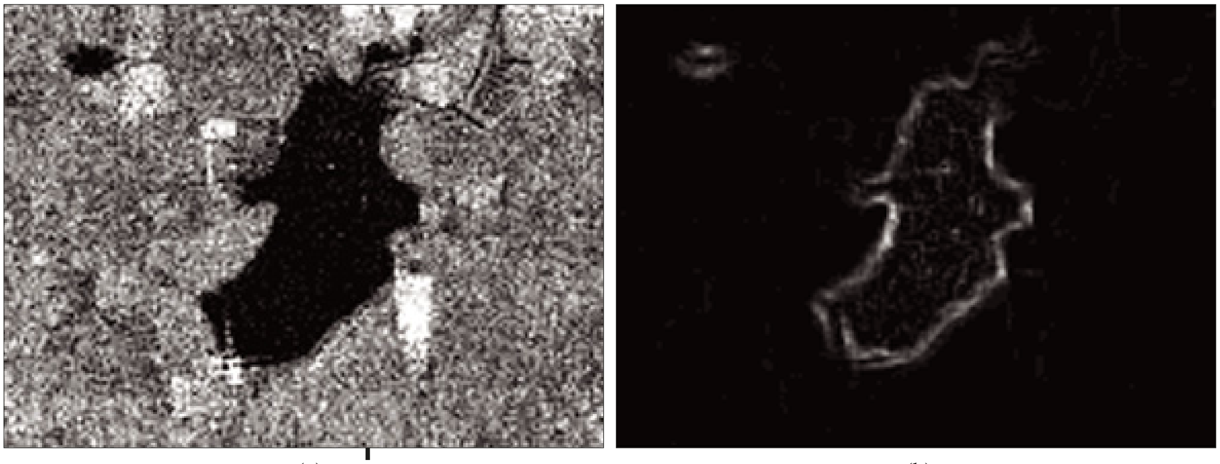

(a) (b)

Figure 1: Water boundaries extracted from a RADARSAT-1 image. (a) Original image; (b) edges detected by the ROEWA operator.

3.2 GAC Model Based on the ROEWA Operator

Ba ROEWA a , a GAC a b a

$$\int_0^{L(C)} g(|r_{max}|)ds + \alpha\int_{\omega} g(|r_{max}|)da \quad (9)$$

g a ba a ROEWA a ,

$$g(|r_{max}|) = \frac{1}{1+|r_{max}|^2/\lambda^2} \quad (10)$$

λ a a a . g b [0, 1], a a a , b . I a , a ba a . A a , a a - a . a a - a a a ,I $a > 0$, a ; - a . a a a a ω C.

T a a a a a a C

$$\frac{\partial C}{\partial t} = [g\kappa + \alpha g - \langle \nabla g, \vec{n}\rangle]\vec{n} \quad (11)$$

A , a ϕ

$$\frac{\partial \phi}{\partial t} = g(\kappa + \alpha)|\nabla\phi| + \nabla g \cdot \nabla\phi \quad (12)$$

where $\kappa = div\left(\frac{\nabla\phi}{|\nabla\phi|}\right)$. To facilitate the numerical a , E . (12) a the property of the divergence $div(\varphi\vec{A}) = \varphi\, div(\vec{A}) + \vec{A}\cdot\nabla\varphi$

$$\frac{\partial \phi}{\partial t} = \left[div\left(g\frac{\nabla\phi}{|\nabla\phi|}\right) + \alpha g\right]|\nabla\phi| \quad (13)$$

4. Implementation

I E . (13). A a a a b a a a . T $div(g\nabla\phi/|\nabla\phi|)|\nabla\phi|$ E . (13) a ab . A a ab a a a a a a , a . I a a ab a a ($\tau < h^2/4$, τ , h a). T , a a ab a b a . H , a a- b a a , a - . O a , AOS ab b a a . T , a .

4.1 Numerical Scheme

T AOS a b *Weickert et al.* [1998] a a a ab a a a $\partial u_0/\partial t = div(g(\nabla u_0)\nabla u_0)$. C a E . (13), a a

ϕ ... (E ...)

$$\phi(x,y)=\begin{cases}-\sqrt{(x-x_0)^2+(y-y_0)^2}, & \text{if } (x,y) \text{ is inside } C\\ 0, & \text{if } (x,y) \text{ is on } C\\ \sqrt{(x-x_0)^2+(y-y_0)^2} & \text{if } (x,y) \text{ is outside } C\end{cases} \quad (14)$$

(x_0, y_0) ... C (... ϕ) ... (x,y), ... $|\nabla\phi| = 1$. C ... , E . (13) b

$$\frac{\partial\phi}{\partial t} = div\,(g\,\nabla\,\phi) + \alpha g \quad (15)$$

E . (15) ... AOS ... *Weickert et al*. [1998].

By defining two matrix operators: $A_1 = \frac{\partial}{\partial x}\left(g\frac{\partial}{\partial x}\right)$, $A_2 = \frac{\partial}{\partial y}\left(g\frac{\partial}{\partial y}\right)$, we can rewrite Eq. (15) as

$$\frac{\partial\phi}{\partial t} = (A_1 + A_2)\phi + \alpha g \quad (16)$$

B ... g ... ROEWA ... A_1 a A_2 . I ... GAC .

L τ b ... , h b ... $(x_i, y_j) = (ih, jh)$ b ... , 1 ... i ... N_x, 1 ... j ... N_y, (N_x a N_y a ...).

Furthermore, let $\sigma^n_{i,j} = \phi(n\tau, x_i, y_j)$ be an approximation ... $\phi(t, x, y)$. T ... ϕ a time $n\tau$ is discretized as a matrix $\left[\phi^n_{ij}\right]_{N_x \times N_y}$. On ... AOS ... . H ... , the matrix $\left[\phi^n_{ij}\right]_{N_x \times N_y}$ should be converted to a col... . I ... ϕ ... $N = N_x \cdot N_y$. T ... g ... . Ba ... , AOS ... E . (16) a ... [*Weickert et al.* 1998; *Goldenberg et al.*2001]

$$\phi^{n+1} = \frac{1}{2}\sum_{l=1}^{2}\left[I - 2\tau A_l\right]^{-1}\left(\phi^n + \tau\alpha g\right) \quad (17)$$

T ... A_l (l = 1, 2) ... E . (17). A ... , $A_l = [a_{l,ij}]_{N\times N}$, ... :

$$a_{l,ij} = \begin{cases}\frac{g_i + g_j}{2h^2}, & j \in N(i)\\ -\sum_{k\in N(i)}\frac{g_i + g_j}{2h^2}, & j = i\\ 0, & else\end{cases} \quad (18)$$

$N(i)$ ... i (b ...) ... . A ... $a_{1,ij}$ a $a_{2,ij}$ a ... . I ... , $N(i)$ ... , $a_{1,ij}$ ... , i − 1 a i + 1; ... , $a_{2,ij}$, $N(i)$ ... , i − N_x a i + N_x. A ... A_l (l = 1,2), ... I − $2\tau A_l$ ... *Thomas algorithm* [*Weickert et al*. 1998].

4.2 Re-initialization of the Level Set Function

A ... ϕ ... $|\nabla\phi| = 1$ ... AOS . H ... . T ... , ϕ ... . T ... . O ... (FM) ... *Sethian* [1996]. T FM ... $O(N \log N)$, ... N ... . R ... , ... *Felzenszwalb and Huttenlocher* [2004] ... *Papandreou and Maragos* [2007]. I ... ϕ ... $O(N)$. F ... , ... H ... , ... T ba ... .

L × = z ... N_x ... 1D ... , a $f : \times \rightarrow R$ ... . T ... E ... 1D ... f ... b

$D_f(x) = \min_{x' \in \Omega} \{(x - x')^2 + f(x')\}$. Note that for each $x' \in \Omega$, a a a a a f b b a a ab a a $(x', f(x'))$. I a , a a b a ab a a a a x . F a (2D) × = z1, , N_x z1, , N_y , 2D a a f a E a a b : D_f (,) $= \min_{x', y' \in \Omega} \{(x - x')^2 + (y - y')^2 + f(x', y')\}$. Note that y' a x', 2D a a - form can be separated, i.e., $D_f(x,y) = \min_{x' \in \Omega} \{(x - x')^2 + D_{f|x'}(y)\}$, where $D_{f|x'}(y) = \min_{y' \in \Omega} \{(y - y')^2 + f(x', y')\}$. T 2D a a b b 1D a a a , a 1D a a a [*Felzenszwalb and Huttenlocher* 2004]. F 2 a a a a a - a a *Felzenszwalb and Huttenlocher* [2004]. T a 512 384 . I a 0.037 b a a .

4.3 Segmentation Algorithm

Ba , a SAR a a a . T a a a a .

S 1, a ϕ^0 (- a) a $n = 0$.

S 2, a g b E . (10).

S 3, a b E . (17) b a a - ϕ^{n+1}.

S 4, a a a a a .

S 5, ϕ^{n+1} a a a . I , , $n = n + 1$ a a .

L ϕ^n a ϕ^{n+1} b A a B, . T $H(A, B)$. T, T a , a , $T = h$ a $H(A, B) =$ a $(h(A, B), h(B, A))$ Ha - tance between A and B. Here $h(B, A) = \max_{a \in A} \min_{b \in B}$ a b Ha A B; a $h(B, A) = \min_{b \in B} \min_{a \in A} \| b - a \|$ is the directed Hausdorff B A. T a a a , a a a a a a a . I E . (5), a a b a a a ROEWA , a SAR a a a . A *Fjortoft et al.* [1998], $a = 0.3$, $b = 0.7$, a SAR a . I E . (10), a a a g, a a g. I r , a , β b a a a . β 0.1 a a . I E . (9), a a a a . I , $a > 0$ a ; a . T a , a . b a a a . H , b [-1, 1] . I a a a b - a , . a a , a a a a a . O a , a a a , . a a a . A a , a b a - a . I E . (18), h a

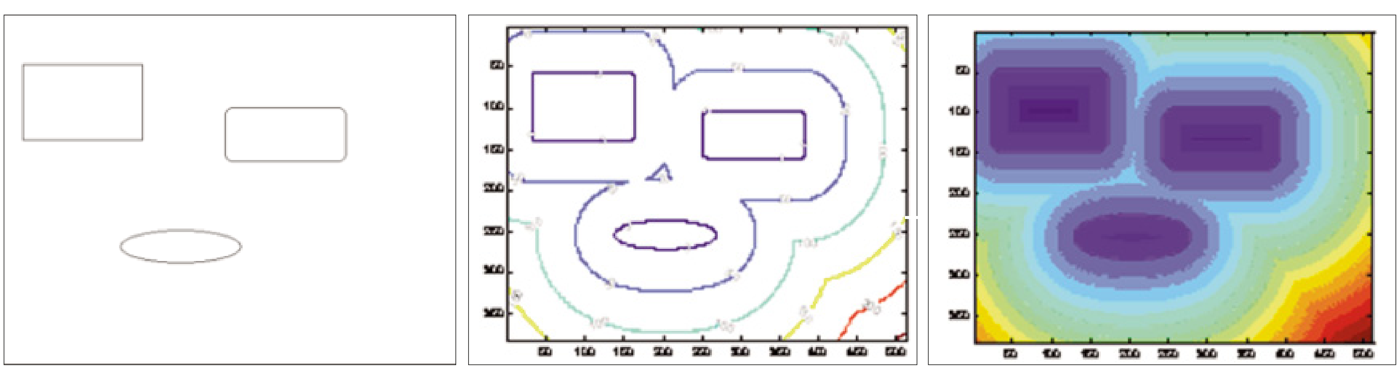

(a) (b) (c)

Figure 2: Signed distance function for a simple image using the distance transform. (a) Simple image. (b) Contours of the signed distance function. (c) Image of the signed distance function.

a . U a , h = 1. I E . (17), τ a . W a b a a a . C a a , b a a a a . U a , τ b a 10.0.

5. Results and Discussion

T a a a RADASAT-2 SAR a a a a . T MATLAB V7.4 a PC a P IV 1.8 GH CPU a 1 GB RAM. T AOS a C++. T a a - a a : b = 0.7, a = 1 b = 0.3, λ = 0.1, h = 1, τ = 5 a ba a a a a a a .

T a a a a - a . T a a a ab a a a a a . T a - a b a a a a b a a . T a b (ENIL) a 1. T a a 256 ˙ 256 a 107 ˙ 100 , . T a a a 41.5497 a 7.204 . T a a b a a a b a . T a a a a 0.68 b

a . T a ab 7.4 a 3.7 . A F 3, b a a a a a . C , a ab a a a .

T RADARSAT-1 a RADARSAT-2 a . T ENIL a 1. T RADARSAT-1 a a a 475 ˙ 350 a 615 ˙ 310 , - a a RADARSAT-2 a a 435 ˙ 342 . T a b a a a 1. T - a RADARSAT-1 a -2 a a 62.0686, 27.0422, 19.8717, 23.3076, 14.4959, 21.5752 a 16.346, . T - a a a a a b a . T a a a a 0.85, 0.80, 0.85, 0.80, 0.83, 0.90 a 0.90, . T RADARSAT-1 a - a ab 13.9 a 20.6 a RADARSAT-2 a a ab 12 , . F 4 a 5 a , a a . T - a a a a - a SAR a . F , a a a , a a a a a a SAR a a . I a , a a a a a a , a a a a a a a S a a .

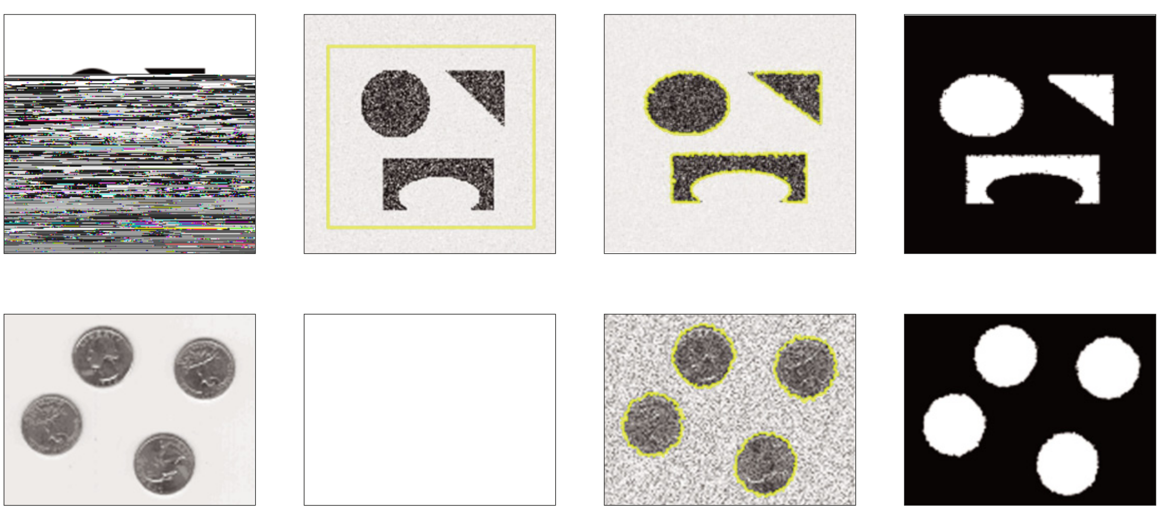

(a) (b) (c) (d)

Figure 3: Segmentation results of two simulated SAR images using our method. (a) Two original optical images. (b) Simulated SAR images with initial contours; (c) Detected contours; (d) Segmentation results.

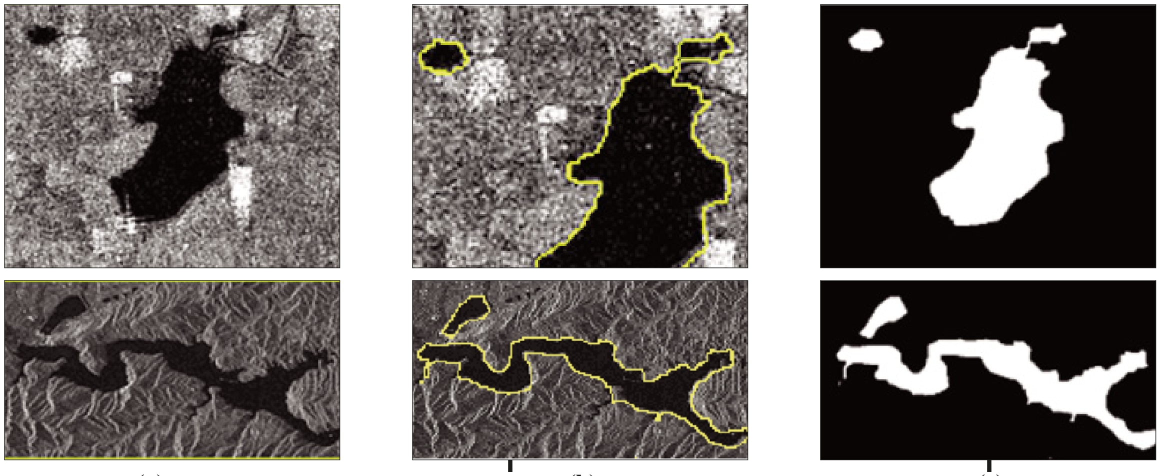

(a) (b) (c)

Figure 4: Segmentation results of two RADARSAT-1 images using our method. (a) Original image extracts with initial contours; (c) Detected contours; (d) Segmentation results.

6. Performance Evaluation

6.1 Quality Evaluation

Ob a a a . - a b a a ba . T a a a a a a a b a a a a . T a a b a a - a b . T a - a b b , a b .

H a *Caves et al.* [1998] a a b a a . *Caves et al*. [1998] a a a a : image σ^2_{RI} and mormalized likelihood ratio of log a a D. S a a u_0, a u_{seg}, a a $m \cdot n$, a a RI a :

$$RI = u_{seg} / u_0 \tag{19}$$

T a a a a a a a , a b a a a . Ba a a , a a a b a :

$$\sigma^2_{RI} = \sum_{k=1}^{L} \frac{n_k}{mn-1}\left(\overline{RI_k^2} - \overline{RI_k}^2\right) \tag{20}$$

$$D = \sum_{k=1}^{L} \frac{n_k}{mn}\left(\ln \overline{RI_k}\right) \tag{21}$$

a L , RI_k b- k- b- b a ,

n_k is the pixel numbers of RI_k, $\overline{RI_k^2}$ and $\overline{RI_k}^2$ are a a a a a RI_k a- a . T a a a - a . T a a a . T a a a a a- a a a a Tab 1.

Table 1: Evaluation results of segmentation quality for two RADARSAT-1 and five RADARSAT-2 images.

RADARSAT-1 a 1		RADARSAT-1 a 2		RADARSAT-2 a 1		RADARSAT-2 a 2		RADARSAT-2 a 3		RADARSAT-2 a 4		RADARSAT-2 a 5	
σ^2_{RI}	D	σ^2_{RI}	D	σ^2_{RI}	D	σ^2_{RI}	D	σ^2_{RI}	D	σ^2_{RI}	D	σ^2_{RI}	D
0.12	0.23	0.11	0.21	0.14	0.23	0.15	0.25	0.12	0.22	0.17	0.24	0.16	0.25

Table 2: Time consumed by the algorithm for images with different sizes.

S ( )	64 · 64	128 · 128	256 · 256	512 · 512	1024 · 1024
T (.)	1.7	6.1	26.5	143.6	864.8

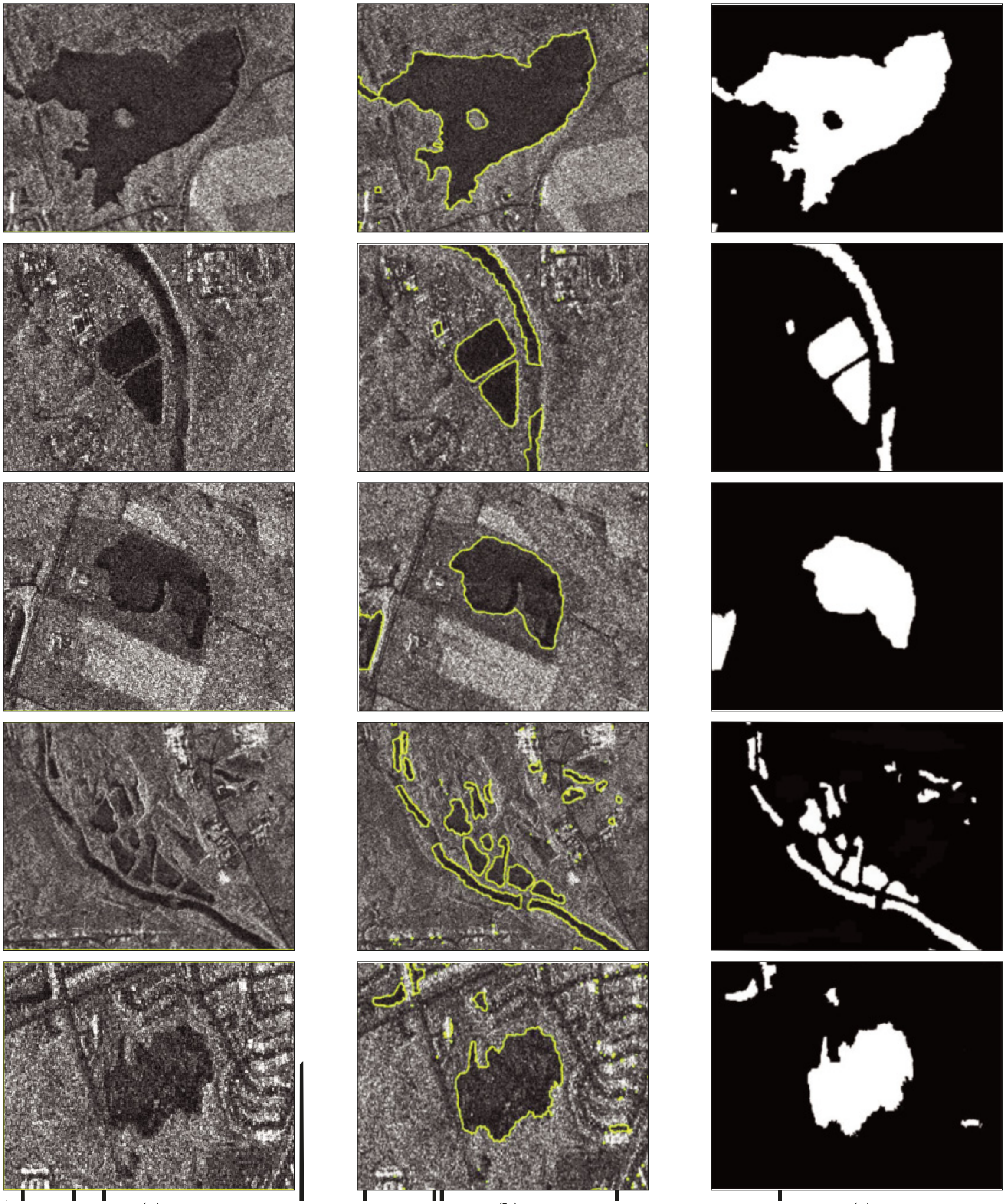

(a) (b) (c)

Figure 5: Segmentation results of five RADARSAT-2 images using our method. (a) Original image extracts with initial contours; (b) Detected contours; (c) Segmentation results.

I a a a a a , - a a . T a a a b a . T a b a a a Tab 2.

6.2 Comparison

I a a a a , a

a a a -ba a ba a a a ([*Fjortoft et al*. 1998] a a), a GAC ba ROEWA (MGAC) .

F 6 -ba a RADARSAT-1 a . Q a a - a a a Tab 3.

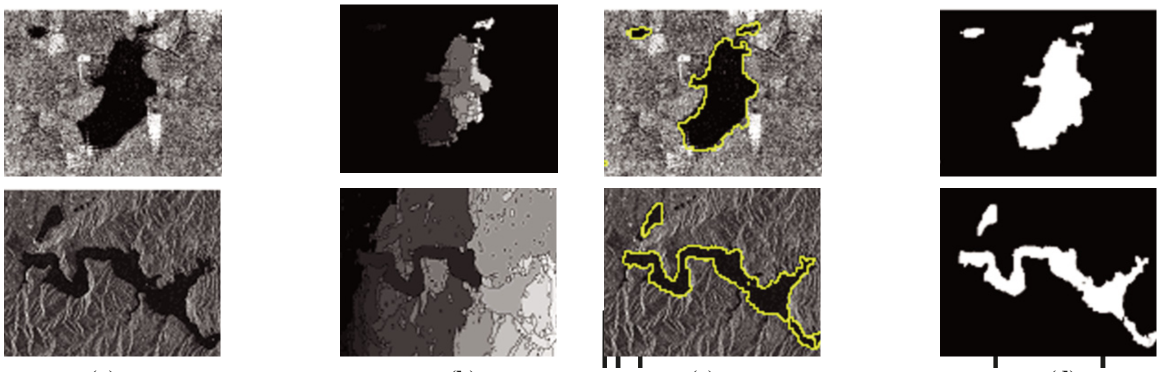

(a) (b) (c) (d)

Figure 6: Segmentation results of the edge-based algorithm. (a) Original images; (b) Results of the watershed algorithm; (c) Detected boundaries; (d) Segmentation results.

Table 3: Quantitative comparison of the two segmentation algorithms.

A	RADARSAT a 1		RADARSAT a 2	
	σ^2_{RI}	D	σ^2_{RI}	D
MGAC	0.12	0.23	0.11	0.21
E -ba	0.27	0.38	0.24	0.35

T a a -
. F , b a ,
b a -ba (a a -
rithm). Secondly, the values of σ^2_{RI} and D from our
a a a a
a (Tab 3),
a a a . T ,
a b a a
a a . I a a , a -
a
a a b a a-
a a a -
ab a a a a -
a . I a , a a
a a - a
.

7. Concluding Remarks

I a , a -
a ba SAR a
-
a . T a b a b
a , a a RADARSAT-1/-2 a
a a a a
a a a a a a a . F ,
a a b a a a
a . S ,
a a a . F a ,
b a a a a S a
a . T , -
, a a a , . D a
a ba

[*Papandreou and Maragos*, 2007]
b a
a . I a , a a
SAR a
a a a

Acknowledgments

T Ca a a I S , E
Ca a a a
RADARSAT a T a a
a a b P . Ga a K a
U Wa . T a
a G Pa a
AOS a a
a ab .

R

B , A C. 1988. O a ,
IEEE Trans. Acoust., Speech Signal Processing, 36(10), . 1618 1627.
Ca , V., R. K , a G. Sa . 1997. G
a , *Int. J. Computer Vision*, 22(1), . 61-79.
C , R., S. Q a , a R. W . 1998. Q a
a a SAR a
a , *IEEE Trans. Image Process*. 7(11), . 1534-1546.
C a , C., V. Pa , a P. R . 1998. R b
a a
a -ba a , *Opt. Lett*., 23(7), . 488 490.
C a , C., P. R , a V. B . 1999. S a a
a -ba a a a
a , *IEEE Trans. Pattern Anal. Machine Intell.*, 21(11), . 1145-1157.
C , L.D. 1991. O a a ba ,
CVGIP: Image Understanding, 53(2), . 211-218.
C , M.J. a E.B. K . 2008. O a
a a b - a SAR
a a a , *IEEE Trans. on Geosc. and Remote Sensing*, 46(6), .1836-1846.
C , R., I. M C , C. O a E. W b .
1994. MUM (M) a

SAR a , *SPIE: SAR Data Processing for Remote Sensing*. . 2316, .92-103.

F a b, P. a D. H . 2004. D a T a Sa F , T a R TR2004-1963. C C . I . S ., C U ., I a a, NY.

F , R., A. L , P. Ma , a E. C. Ca a . 1998. A a SAR a a , *IEEE Trans. Geosci. Remote Sensing*, 36(3), . 793-802.

F , R., Y. D , W. P , a F. T . 2003. U a a a a a Ma a a Ma a , *IEEE Trans. Geosci. Remote Sensing*, 41(3), . 675-686.

G a , O. a P. R . 2001. E a SAR a : a a - a a a a a a , *IEEE Trans. Image Process.*, 10(1), . 72-78.

G b , R., R. K , E. R , a M. R . 2001. Fa a , *IEEE Trans. Image Process.*, 10(10), . 1467-1475.

H , Z, L , J, a G. K a G. 2009. SAR a - a ba ba a , *Progress in Nature Science*, 10(3), . 344-360.

Ka , M., A. W , a D. T . 1988. S a : a , *Int. J. Computer Vision*, 1(4), . 321-331.

Ma , P., P. R , F. G a , a F. G a . 2004. I a - a , *IEEE Trans. Pattern Anal. Machine Intell.* 26(6), . 799-803.

O , C.J., D. B a a R.G. W . 1996. O a SAR, *IEEE Proc. Radar, Sonar Naving*. 143(1) . 31-40.

O , S., a J.A. S a . 1998. F a a a - : a ba Ha -Ja b a , *J. Computational Physics*. 79(1), . 12-49.

Pa a , G. a F. Ma a . 2007. M - a , *IEEE Trans. Image Process.*, 16(1), . 229-240.

S , G.A., a E.T. E a . 2000. *Remote Sensing in Hydrology and Water Management*, S - V a , B , G a .

S a , J. A. 1996. A a a a a , *Proc. National Academic Science*, 93(4), 1591-1595.

S , J. a S. Ca a . 1992. A a a a , *CVGIP: Graph., Models, Image Process.*, 54(2), . 12 133.

S , Y. M., J. L , a G. G . 2010. S a - RADARSAT-2 a a a ba a a a , *Marine Geodesy*, 33(2&3), . 187-203.

T , R., A. L , a P. B - . 1988. A a a a a SAR a , *IEEE Trans.Geosci. Remote Sensing*, 26(6), . 764-773.

W , J., B. R , a M. V . 1998. E a ab a - , *IEEE Trans. Image Process.*, 7(3), . 398-410.

Z , S.C. a A. Y . 1996. R : - a , , a B /MDL ba a a , *IEEE Trans. Pattern Anal. Machine Intell*. 18(9), . 884-900.

Authors

Dr. Gangyao Kuang B.S . a M.S . C a S U , C a, 1988 a 1991, , a P .D. Na a U D T (NUDT), C a, 1995. S 1996, a b C - R S I a P Lab a a NUDT, a b SAR a a a - , a a a a , a a a a - . H a P S E S a E a NUDT. H a / a 200 a a b . H , SAR a , a , SAR a a , a a a- a SAR a .

Dr. Jonathan Li P .D. - a U Ca T , S A a a a a a a D a G a & E a Ma a a a a R S a G a a T a a U Wa , Ca a a. H a A P Y U , P U , W a U , T a U , H a U , C a a U , C a S U a C a U G . H a b 150 b a - b a 5 a a a a 60 - a a . H a SAR SAR a a- , a a , b a a a RADARSAT a a a a a a a a a . D . L V C a ICA C Ma Sa I a a a A a E *Geomatica*.

Dr. Zhiguo He B.S ., M.S ., a P .D. Na a U D T , C a a, C a, 2001, 2004 a 2008, . a a . H a - SAR a , a a a SAR a . ❑